AIP | Applied Physics Letters

# Real-time observation of phonon-polariton dynamics in ferroelectric LiNbO3 in time-frequency space

Yuki Ikegaya, Hiroyuki Sakaibara, Yasuo Minami, Ikufumi Katayama, and Jun Takeda

Citation: Applied Physics Letters **107**, 062901 (2015); doi: 10.1063/1.4928480
View online: http://dx.doi.org/10.1063/1.4928480
View Table of Contents: http://scitation.aip.org/content/aip/journal/apl/107/6?ver=pdfcov
Published by the AIP Publishing



# Real-time observation of phonon-polariton dynamics in ferroelectric $LiNbO_3$ in time-frequency space

Yuki Ikegaya, Hiroyuki Sakaibara, Yasuo Minami, Ikufumi Katayama, and Jun Takeda[a)]
*Department of Physics, Graduate School of Engineering, Yokohama National University, Yokohama 240-8501, Japan*

(Received 1 July 2015; accepted 30 July 2015; published online 10 August 2015)

We demonstrate the real-time observation of phonon-polariton propagation in ferroelectric $LiNbO_3$ using a single-shot spectroscopic setup that employs an echelon mirror. The echelon mirror provides a spatially encoded time delay for the probe pulse; therefore, the ultrafast transient behavior of materials can be detected on a single-shot basis. Using optical Kerr gate apparatus, forward and backward propagating *E*-mode phonon-polaritons were simultaneously induced via an impulsive stimulated Raman scattering process, and subsequently, their dynamics were readily mapped in time-frequency space using heterodyne detection. The two phonon-polaritons appeared on opposite sides of the central probe wavelength and were symmetrically imaged against the ordinary and extraordinary probe lights. By taking into account coupling of the lowest *E*-mode phonon-polariton to a low-frequency relaxational mode, not only the phonon-polariton dispersion but also the wavevector dependence of the damping rate was unveiled and quantitatively evaluated. © *2015 AIP Publishing LLC*. [http://dx.doi.org/10.1063/1.4928480]

Ferroelectric materials are of great interest for use in various types of nonlinear optical applications such as harmonic generation and electro-optic modulators. Furthermore, intense terahertz (THz) generation at more than 1 MV/cm has been recently realized using ferroelectric $LiNbO_3$.[1–3] Under intense THz field illuminations, the nonlinear and anharmonic properties of materials have been demonstrated, such as THz-field-induced anharmonicity of the ferroelectric soft mode in $SrTiO_3$,[4] THz-field-induced photovoltaic effects in $LiNbO_3$,[5] resonant and non-resonant material control,[6] and nonlinear electron delocalization.[7] Therefore, it has become increasingly important to elucidate both the linear and nonlinear characteristics of light-induced lattice vibrations (phonon-polaritons) that are observed in the THz frequency region in ferroelectric materials.

Although the spatiotemporal characteristics of phonon-polaritons have been studied via sophisticated time-domain measurements,[8–10] information is still required on their dynamic behavior in time-frequency space; this is necessary to develop a fundamental understanding of the phonon-polaritons. Multidimensional spectroscopy will become a key technique to overcome this limitation;[11] in this context, we have developed a single-shot time-frequency two-dimensional (2D) imaging spectroscopic method,[12–14] which enables the time-frequency 2D mapping of ultrafast transients on a single-shot basis. Recent use of this technique led to the single-shot observation of irreversible amorphization processes in phase-change chalcogenide alloy thin films ($Ge_2Sb_2Te_5$).[15] In this letter, we report the real-time observation of phonon-polariton propagations in ferroelectric $LiNbO_3$. This work showcases not only the dispersion relation of the anisotropic *E*-mode phonon-polaritons but also the wavevector dependence of the damping rate, which was unveiled via real-time monitoring in time-frequency space.

Figure 1 shows the experimental setup used in this study. Using a four-focusing configuration, a reflective echelon mirror with 500 steps acted as a spatially encoded time delay optic for the probe pulses; each step had a step-width of 20 $\mu$m and a step-height of 5 $\mu$m, yielding a temporal step and a total time delay of 34 fs and 17 ps, respectively. The optical setup of our single-shot spectroscopy is described in detail elsewhere.[13] We used a Ti:sapphire regenerative amplifier with a 1 kHz repetition rate, a 795 nm central wavelength, and a pulse duration of 130 fs. The amplifier output was divided by a beam splitter (BS) into two beams: the

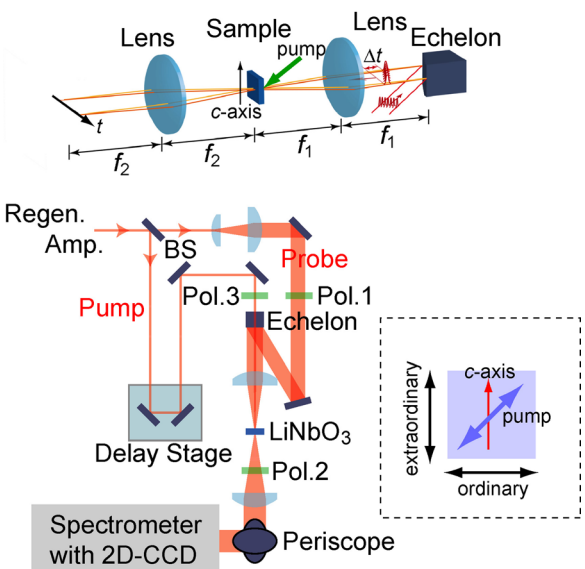


FIG. 1. Schematic of single-shot imaging spectroscopy. The inset in the dashed square illustrates the polarization directions of the pump and probe beams relative to the *c*-axis of the $LiNbO_3$ thin plate. BS: beam splitter and Pol: polarizer.

[a)]Author to whom correspondence should be addressed. Electronic mail: jun@ynu.ac.jp.

 

intense pump (70%) and probe (30%) beams. The pump pulse and the probe beam with a spatially encoded time delay were focused on an *x*-cut $LiNbO_3$ thin plate (1 mm thickness). After passing through the sample, the transmitted probe was precisely imaged onto the entrance slit of a spectrometer with a 2D charge coupled device (CCD) detector to obtain a time-frequency 2D image of the ultrafast responses of $LiNbO_3$. The polarization of the pump was set to 45° with respect to the $LiNbO_3$ crystal *c*-axis, while that of the probe was oriented along either the ordinary or extraordinary light direction. Using an optical Kerr gate configuration, an anisotropic *E*-mode phonon-polariton could be induced via an impulsive stimulated Raman scattering (ISRS) process.[16–19] By tilting the second polarizer slightly away from the crossed configuration of a set of two polarizers (Pol. 1 and Pol. 2), we were able to detect phonon-polariton oscillations via heterodyne detection.[20] When evaluating the time resolution of our optical setup, we measured the instantaneous electronic response of the $LiNbO_3$ crystal itself using the completely crossed configuration via the optical Kerr effect.[21] The time resolution was estimated to be approximately 150 fs. This time resolution allowed us to pump and probe only the lowest *E*-mode phonon-polariton ($\leq$4 THz).

Figure 2(a) shows time-wavelength 2D images indicating the ultrafast responses of the extraordinary and ordinary probe lights. Although the 2D image could be obtained even with a single-shot detection, these images were averaged over 100 laser shots (100 ms) to precisely evaluate wavelength-dependent physical quantities such as phonon-polariton frequency and damping constant. Following an instantaneous electronic response at time $t = 0$, oscillations due to the *E*-mode phonon-polariton were clearly observed for both polarizations. The electronic response disappears at shorter wavelength region in case of the ordinary probe light, whose reason is unclear yet. Fourier transformed spectra of the oscillatory components are shown in Fig. 2(b). As indicated by the dashed ovals in Fig. 2(b), the two phonon-polariton modes that appeared at approximately 3 and 4 THz are symmetric about the central wavelength (795 nm) of the laser pulses for each probe polarization. The mesh-like unessential artifacts appeared in Fig. 2(b) might be due to the interference between the probe and crosstalk stray lights. The temporal behaviors of the oscillatory components of the ordinary probe light at different wavelengths, which were obtained from slices of the observed 2D image, are shown in Fig. 2(c). The temporal profile at shorter and longer probe wavelengths can be described by a damped harmonic oscillation, whereas that around the central wavelength shows a modulation between the two modes at approximately 3 and 4 THz in Fig. 2(b). Note that the observed dephasing time of the shorter wavelength (~1.7 ps) is slower than that of the longer wavelength (~1.3 ps). Figure 2(d) displays the time evolutions of the instantaneous electronic responses for the ordinary probe light under the completely crossed and heterodyne configurations. The electronic response measured via the heterodyne detection shows a decay profile after time $t = 0$, implying the existence of a low-frequency relaxational mode.[22]

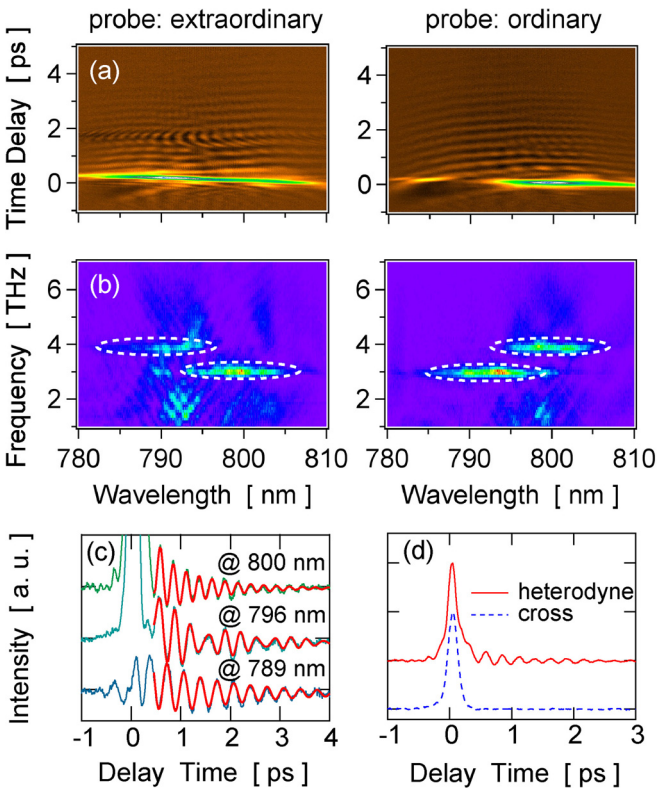


FIG. 2. (a) Time-wavelength 2D images of ultrafast responses in $LiNbO_3$ for the extraordinary and ordinary probe lights. (b) Fourier transformed spectra of the oscillatory components in (a). The dotted ovals indicate the *E*-mode phonon-polaritons induced by ISRS. (c) Time evolutions of the phonon-polaritons at different probe wavelengths for the ordinary probe light. The solid curves show the lines of best fit to the experimental data, using the expression for equation $f(t)$ defined in the text. (d) Temporal profiles of the electronic responses at 800 nm probe wavelength under the completely crossed and heterodyne configurations.

In order to explain these results qualitatively, the pump and probe processes of the *E*-mode phonon-polariton via ISRS, together with the dispersion relations of the phonon-polariton, are schematically displayed in Fig. 3. In case of the pump process, since the refractive index of $LiNbO_3$ differs in the extraordinary (e) and ordinary (o) directions, the two-phase-matched phonon-polaritons can be simultaneously induced via ISRS: backward and forward propagating phonon-polaritons with opposite propagation directions (Fig. 3(a)). Because of the broad spectrum of the laser pulses (indicated by crosshatched areas in Fig. 3), each of these forms a wavepacket with different wavevectors (indicated by dashed circles). When probing the phonon-polariton with ordinary light, as shown in Fig. 3(b), the low frequency ($\Omega_-$) backward propagating phonon-polariton appears at a shorter wavelength, due to the sum-frequency generation ($\omega^{(o)}_{probe} + \Omega_-$), while the high frequency ($\Omega_+$) forward propagating phonon-polariton emerges at a longer wavelength, due to the difference-frequency generation ($\omega^{(o)}_{probe} - \Omega_+$). In contrast, when probing phonon-polariton propagation with extraordinary light, these two modes are observed in the opposite conditions: the backward propagating phonon-polariton appears at a longer wavelength due to the difference-frequency generation ($\omega^{(e)}_{probe} - \Omega_-$), while the forward propagating phonon-polariton emerges at a shorter wavelength due to sum-frequency generation ($\omega^{(e)}_{probe} + \Omega_+$). Therefore, the two phonon-polariton modes located at approximately 3 and 4 THz are symmetrically

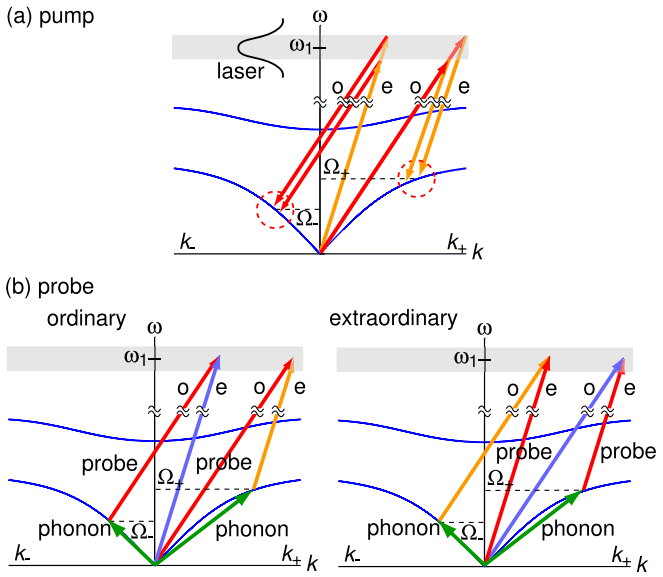


FIG. 3. Schematic of the pump and probe processes of an anisotropic *E*-mode phonon-polariton in $LiNbO_3$. (a) Phase-matched backward and forward propagating phonon-polaritons with different phonon frequencies ($\Omega_-$, $\Omega_+$) and wavevectors ($k_-$, $k_+$) can be simultaneously driven via ISRS using the extraordinary (e) and ordinary (o) light components of pump pulses. (b) Backward and forward propagating phonon-polaritons can be detected via the sum-frequency and difference-frequency generation processes, respectively, for ordinary probe light, while this relation is reversed for the case of extraordinary probe light.

imaged about the central wavelength of the laser pulses in time-wavelength space, as shown in Fig. 2(b).

Next, we quantitatively discuss the dispersion relation and fast dephasing time of the *E*-mode phonon-polariton observed in our experiments. Note that the propagation or escape of the *E*-mode phonon-polariton away from the detected area does not contribute to the observed fast dephasing time. In ferroelectric $LiTaO_3$, an anomalous high damping rate was observed for the lowest frequency $A_1$ phonon-polariton via ISRS measurements. In order to explain this high damping rate, coupling of the polariton to a weakly Raman-active low-frequency relaxational mode was suggested.[22] Since the ferroelectric properties of $LiNbO_3$ are similar to those of $LiTaO_3$, here we apply the same formalism to the *E*-mode phonon-polariton in $LiNbO_3$. The dispersion relation can be derived from the following equations of motion, by taking into account bilinear coupling of the lowest polar optic mode to a relaxational mode:

$$\frac{d^2\boldsymbol{q}(t)}{dt^2}+\Gamma\frac{d\boldsymbol{q}(t)}{dt}+\omega_{\mathrm{TO}}^2\boldsymbol{q}(t)=a_{12}\boldsymbol{E}(t)+a_{1r}\boldsymbol{q}_r(t), \quad (1)$$

$$\tau\frac{d\boldsymbol{q}_r(t)}{dt}+\boldsymbol{q}_r(t)=a_{r1}\boldsymbol{q}(t), \quad (2)$$

$$\boldsymbol{p}(t)=a_{21}\boldsymbol{q}(t)+a_{22}\boldsymbol{E}(t). \quad (3)$$

Here, $\boldsymbol{q}(t)$ is the vibrational coordinate, $\boldsymbol{E}(t)$ is the electric field, $\tau$ is the decay time of the relaxational mode, $\boldsymbol{p}(t)$ is the polarization, and the $a$'s are the coupling constants: $a_{12}a_{21}=\omega_{\mathrm{TO}}^2\varepsilon_0[\varepsilon_0-\varepsilon_\infty]$, $a_{22}=\varepsilon_0[\varepsilon_\infty-1]$, and $a_{1r}a_{r1}$ is the coupling of the lowest polar optic mode to a relaxational mode, where $\varepsilon_0$ and $\varepsilon_\infty$ are the low and high frequency dielectric constants. By removing the coupling constant of $a_{1r}a_{r1}$, the formalism is reduced to a harmonic oscillator model, where $\omega_{\mathrm{TO}}$ and $\Gamma$ are the natural frequency and decay rate, respectively, of the pure transverse mode.[16,22] On the other hand, under the phase-matching condition, the wavevectors for backward and forward propagating phonon-polaritons, $k_-$ and $k_+$, can be expressed by the following expressions:

$$k_-=\frac{n_{\mathrm{e}}}{c}\omega_1-\frac{n_{\mathrm{o}}}{c}(\omega_1-\Omega_-), \quad (4)$$

$$k_+=\frac{n_{\mathrm{o}}}{c}\omega_1-\frac{n_{\mathrm{e}}}{c}(\omega_1-\Omega_+), \quad (5)$$

where $n_{\mathrm{e}}$ (=2.18) and $n_{\mathrm{o}}$ (=2.26) are the refractive indices of $LiNbO_3$ for the extraordinary and ordinary lights, respectively, $\omega_1$ is the laser frequency, $c$ is the speed of light, and $\Omega_-$ and $\Omega_+$ are the lowest polariton frequencies with different wavenumbers. Using previously determined physical parameters for $LiNbO_3$ of $\omega_{\mathrm{TO}}=152\,\mathrm{cm}^{-1}$, $\omega_{\mathrm{LO}}=198\,\mathrm{cm}^{-1}$, $\Gamma=14\,\mathrm{cm}^{-1}$, and $\varepsilon_\infty=22.5$,[23,24] together with the observed relaxational mode decay time of $\tau=0.26\pm0.06$ ps, which was estimated using the slope of the electronic response after

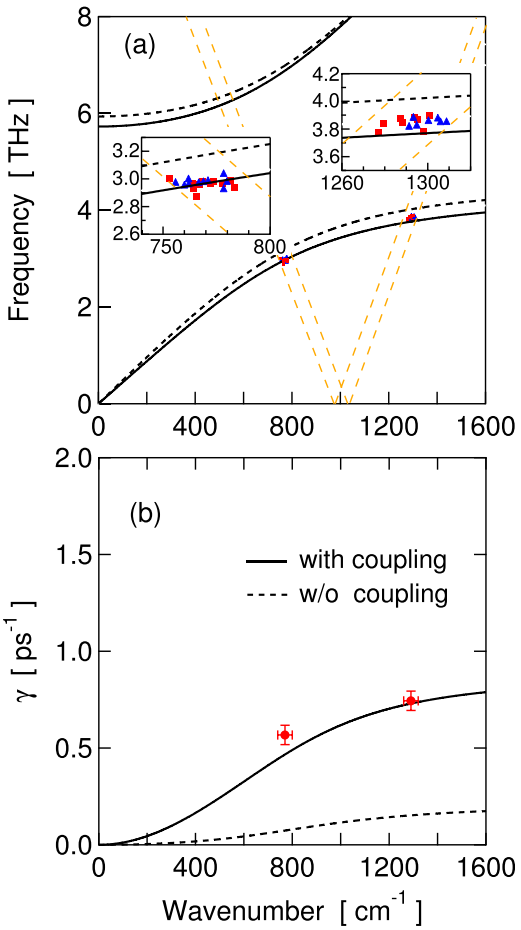


FIG. 4. (a) Estimated dispersion relation and (b) wavevector-dependent damping rate of the lowest *E*-mode phonon-polariton with and without bilinear coupling. The coupling constant was set to $a_{1r}a_{r1}=10^4\,\mathrm{cm}^{-2}$ in order to reproduce the experimental results. The insets show the intersection areas between the dispersion curves and the upper and lower limits of the phase-matching conditions. All data obtained for the ordinary (triangles) and extraordinary (squares) probe lights, which came from the wavelength-resolved phonon-polariton frequencies observed in Fig. 2(b), lie within these areas.

time $t = 0$ (Fig. 2(d)), we can predict the dispersion relation and wavevector-dependent damping rate of the lowest *E*-mode phonon-polariton in $LiNbO_3$.

The estimated dispersion relation and wavevector-dependent damping rate with a coupling constant of $a_{1r}a_{r1} = 10^4\,cm^{-2}$, whose value is almost equal to that of $LiTaO_3$,[22] are indicated by solid curves in Figs. 4(a) and 4(b), respectively. Dashed curves indicate results obtained without coupling. The upper and lower limits of the phase-matching conditions are indicated with dashed lines in Fig. 4(a), and the intersection areas are magnified in the insets. As shown in Figs. 4(a) and 4(b), the experimental data are well reproduced by this model. According to the model, the temporal behavior of the phonon-polariton, $f(t)$, is given by $f(t) = A\exp(-\gamma_{\pm}t)\sin(\Omega_{\pm}t + \phi) + B\exp(-t/\tau)$. By substituting the obtained values of $\gamma_{\pm}$ ($\gamma_+ = 0.77$ ps$^{-1}$ and $\gamma_- = 0.59$ ps$^{-1}$), $\Omega_{\pm}$ ($\Omega_+ = 3.85$ THz and $\Omega_- = 2.98$ THz), and $\tau$ into this equation, the time evolution of the phonon-polariton can be also well reproduced, as shown by the solid curves in Fig. 2(c). These results indicate that the inclusion of bilinear coupling between the lowest polar optic mode and a relaxational mode is indispensable in a quantitative discussion of the *E*-mode phonon-polariton dynamics in $LiNbO_3$.

In conclusion, we demonstrated the real-time observation of phonon-polariton propagations in ferroelectric $LiNbO_3$ using single-shot spectroscopy with an echelon mirror. Optical Kerr gate apparatus and heterodyne detection were employed in order to evaluate anisotropic *E*-mode phonon-polariton dispersion in real-time. By considering coupling of the lowest polar optic mode to a low-frequency relaxational mode, the dispersion relation and the wavevector dependence of the damping rate were revealed and quantitatively defined. We expect that our single-shot spectroscopy method will be widely utilized in unveiling various types of ultrafast phenomena via real-time monitoring in time-frequency space.

This work was supported in part by the Grants-in-Aid for Scientific Research (Grant Nos. 23241034, 25800177, 26107517, and 15K13273) from the Japan Society for the Promotion of Science and the Ministry of Education, Culture, Sports, Science, and Technology.

[1]J. Hebling, G. Almási, and Z. I. Kozma, Opt. Express **10**, 1161 (2002).
[2]J. A. Fülöp, L. Pálfalvi, G. Almási, and J. Hebling, Opt. Express **18**, 12311 (2010).
[3]H. Hirori, A. Doi, F. Blanchard, and K. Tanaka, Appl. Phys. Lett. **98**, 091106 (2011).
[4]I. Katayama, H. Aoki, J. Takeda, H. Shimosato, M. Ashida, R. Kinjo, I. Kawayama, M. Tonouchi, M. Nagai, and K. Tanaka, Phys. Rev. Lett. **108**, 097401 (2012).
[5]C. Somma, K. Reimann, C. Flyzanis, T. Elsaesser, and M. Woerner, Phys. Rev. Lett. **112**, 146602 (2014).
[6]T. Kampfrath, K. Tanaka, and K. A. Nelson, Nat. Photonics **7**, 680 (2013).
[7]K. Yoshioka, Y. Minami, K. Shudo, T. D. Dao, T. Nagao, M. Kitajima, J. Takeda, and I. Katayama, Nano Lett. **15**, 1036 (2015).
[8]R. M. Koehl, S. Adachi, and K. A. Nelson, J. Phys. Chem. A **103**, 10260 (1999).
[9]N. S. Stoyanov, D. W. Ward, T. Feurer, and K. A. Nelson, Nat. Mater. **1**, 95 (2002).
[10]K. Nakagawa, A. Iwasaki, Y. Oishi, R. Horisaki, A. Tsukamoto, A. Nakamura, K. Hirosawa, H. Liao, T. Ushida, K. Goda, F. Kannari, and I. Sakuma, Nat. Photonics **8**, 695 (2014).
[11]S. M. Teo, B. K. Ofori-Okai, C. A. Werley, and K. A. Nelson, Rev. Sci. Instrum. **86**, 051301 (2015).
[12]N. Furukawa, C. M. Mair, V. D. Kleiman, and J. Takeda, Appl. Phys. Lett. **85**, 4645 (2004).
[13]I. Katayama, H. Sakaibara, and J. Takeda, Jpn. J. Appl. Phys., Part 1 **50**, 102701 (2011).
[14]Y. Minami, H. Yamaki, I. Katayama, and J. Takeda, Appl. Phys. Express **7**, 022402 (2014).
[15]J. Takeda, W. Oba, Y. Minami, T. Saiki, and I. Katayama, Appl. Phys. Lett. **104**, 261903 (2014).
[16]T. P. Dougherty, G. P. Wiederrecht, and K. A. Nelson, J. Opt. Soc. Am. B **9**, 2179 (1992).
[17]H. J. Bakker, S. Hunsche, and H. Kurz, Phys. Rev. B **50**, 914 (1994).
[18]C.-C. Lee, C.-T. Chia, Y.-M. Chang, M. L. Sun, and M.-L. Hu, Jpn. J. Appl. Phys., Part 1 **43**, 6829 (2004).
[19]O. Albert, C. A. Gautier, J. C. Loulergue, and J. Etchepare, Solid State Commun. **107**, 567 (1998).
[20]H. Sakaibara, Y. Ikegaya, I. Katayama, and J. Takeda, Opt. Lett. **37**, 1118 (2012).
[21]J. Takeda, K. Nakajima, S. Kurita, S. Tomimoto, S. Saito, and T. Suemoto, Phys. Rev. B **62**, 10083 (2000).
[22]G. P. Wiederrecht, T. P. Dougherty, L. Dhar, K. A. Nelson, D. E. Leaird, and A. M. Weiner, Phys. Rev. B **51**, 916 (1995).
[23]A. S. Barker and R. Laudon, Phys. Rev. **158**, 433 (1967).
[24]S. Kojima, N. Tsumura, H. Kitahara, M. W. Takeda, and S. Nishizawa, Jpn. J. Appl. Phys., Part 1 **41**, 7033 (2002).